Development of blade element momentum (BEM) method for hydropower

Downloaded from: https://research.chalmers.se, 2024-04-09 04:56 UTC

Citation for the original published paper (version of record):
Abedi, H., Ibáñez Uribe, C., Fahlbeck, J. et al (2022). Development of blade element momentum (BEM) method for hydropower. IOP Conference Series: Earth and Environmental Science, 1079(1). http://dx.doi.org/10.1088/1755-1315/1079/1/012014

N.B. When citing this work, cite the original published paper.

research.chalmers.se offers the possibility of retrieving research publications produced at Chalmers University of Technology. It covers all kind of research output: articles, dissertations, conference papers, reports etc. since 2004. research.chalmers.se is administrated and maintained by Chalmers Library

(article starts on next page)

PAPER • OPEN ACCESS

Development of blade element momentum (BEM) method for hydropower

To cite this article: H Abedi *et al* 2022 *IOP Conf. Ser.: Earth Environ. Sci.* **1079** 012014

View the article online for updates and enhancements.

You may also like

- Comparison of aerodynamic planform optimization of non-planar rotors using blade element momentum method and a vortex cylinder model
Ang Li, Mac Gaunaa, Kenneth Lønbæk et al.
- Integral equations and boundary-element solution for static potential in a general piece-wise homogeneous volume conductor
Matti Stenroos
- Comparative performance of the finite element method and the boundary element fast multipole method for problems mimicking transcranial magnetic stimulation (TMS)
Aung Thu Htet, Guilherme B Saturnino, Edward H Burnham et al.

This content was downloaded from IP address 129.16.140.129 on 17/10/2022 at 12:23

Development of blade element momentum (BEM) method for hydropower

H Abedi, C I Uribe, J Fahlbeck and H Nilsson

Division of Fluid Dynamics, Department of Mechanics and Maritime Sciences, Chalmers University of Technology, SE-412 96, Gothenburg, Sweden

E-mail: hamidreza.abedi@chalmers.se

Abstract. The BEM method is extensively used for analyzing the aerodynamic performance of wind turbines and marine propellers. It is computationally fast and is easily implemented while it can give fairly accurate results. Application of the BEM method to predict the forces acting on rotor blades for a model scale axial shaft-driven Counter-Rotating Pump-Turbine (CRPT) is investigated. Some modifications have been proposed to adopt the classical BEM method for CRPT machine and the results are validated against results from Computational Fluid Dynamics (CFD). The results display that the proposed modifications can improve the loading predicted by BEM. However, the improvements are more pronounced in pump mode rather than turbine mode.

1. Introduction

The imbalance between supply and demand in an electrical system can be treated by different techniques ranging from electrical power stations to store surplus electricity at low demand instances and release at high demand periods. Pumped Hydro Storage (PHS) can be an appropriate solution for electric load balance which can be done using Reversible Pump-Turbines (RPTs). Various numerical modeling techniques with different levels of complexity and accuracy may be used to simulate the flow through RPTs. For design purpose, numerous simulations covering an extensive range of operating conditions must be performed. Computational Fluid Dynamics (CFD), solving the Navier-Stokes equations for the flow around the rotor blades, is known as the most accurate but computationally most expensive method. Therefore, it is of interest to develop a computationally faster method by reducing the flow complexity.

Today, an engineering model based on the Blade Element Momentum (BEM) method is extensively used for analyzing the aerodynamic performance of wind turbines. It is known as the improved model of the Rankine-Froude momentum theory [1, 2], which was the first model to predict inflow velocities at the rotor. Compared to the high-fidelity CFD models, the BEM method is less accurate because of several assumptions and simplifications. However, it is computationally much cheaper than CFD and is still useful as an engineering method to predict the loads on the rotor blades. In this paper, the classical BEM method is adapted to assess the performance of a Counter-Rotating Pump-Turbine (CRPT) in terms of the total thrust T, torque Q and power P for any combination of incoming volumetric flow q and rotational speed of the rotors n. The results are validated against CFD simulations. Figure 1 demonstrates a schematic view of a CRPT machine with two counter-rotating runners inside the guiding pipe

Content from this work may be used under the terms of the Creative Commons Attribution 3.0 licence. Any further distribution of this work must maintain attribution to the author(s) and the title of the work, journal citation and DOI.
Published under licence by IOP Publishing Ltd

where water can flow in any direction depending on the prescribed operating modes (pump or turbine).

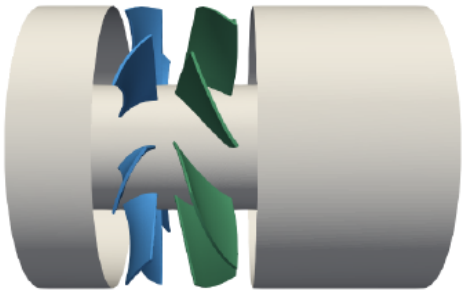

Figure 1. Schematic of CRPT concept including runner 1 (blue) and runner 2 (green).

2. Methods

2.1. Classical Blade Element Momentum (BEM) Theory

The classical Blade Element Momentum (BEM) Method was introduced by Glauert [3] in 1935 to design and analyse rotor blades. The BEM method combines the Blade Element Theory and the Momentum Theory [4, 5]. In the BEM method, forces acting on a blade element are estimated as the forces on an airfoil of the same cross-section (using tabulated two-dimensional airfoil data) which advances through the fluid with the uniform velocity at an angle of attack along with 1D momentum theorem. According to 1D axial momentum theory, based on the ideal representation of the rotor blades the so-called actuator disk [4], the differential form of the thrust and the torque acting over an annular cross section area $\mathrm{dA} = 2\pi r\mathrm{dr}$ within the actuator disk can be computed by

$$\mathrm{dT} = 2\rho U_0^2 a(1-a)\mathrm{dA} = 4\pi\rho U_0^2 a(1-a)r\mathrm{dr}, \tag{1}$$

where r, dr and U_0 are the radial distance of any annular element of the rotor blade, thickness of annular element and freestream velocity, respectively. The axial induction factor a represents a percentage of the axial flow decelerated at the rotor plane with respect to the far upstream flow. By extending the axial momentum theory to involve the effects of the rotational motion of the actuator disk rotating with the angular velocity using the general momentum theory [6], an expression for the differential torque is obtained. The angular momentum balance in an annular element of the rotor blade gives the differential torque written as

$$\mathrm{dQ} = ru_\theta \mathrm{d}\dot{m} = 4\pi\rho U_0 \Omega a'(1-a)r^3\mathrm{dr}, \tag{2}$$

where $\mathrm{d}\dot{m} = \rho u_R 2\pi r\mathrm{dr}$ and a' denote the differential mass flow passing through the disk region and tangential induction factor, respectively. The axial (a) and tangential (a') induction factors are obtained from axial and angular momentum balance in an annular element of the rotor blade, respectively [4]. Employing blade-element theory, which assumes that each rotor blade element operates independently of all other elements, thrust (due to axial loading) and torque (due to tangential loading) on the control volume of thickness dr can be written as

$$\mathrm{dT} = ZF_n\mathrm{dr} = \frac{1}{2}\rho Zc V_{rel}^2 C_n\mathrm{dr} \quad , \quad C_n = C_l\cos(\phi) + C_d\sin(\phi). \tag{3a}$$

$$\mathrm{dQ} = rZF_t\mathrm{dr} = \frac{1}{2}\rho Zc V_{rel}^2 C_t\mathrm{dr} \quad , \quad C_t = C_l\sin(\phi) - C_d\cos(\phi), \tag{3b}$$

where Z, F_n, F_t, c, C_n and C_t are the number of blades, axial force to the rotor plane (per blade element length), tangential force to the rotor plane (per blade element length) to the rotor plane, the local blade chord, 2D axial force coefficient and 2D tangential force coefficient, respectively. The 2D axial and tangential force coefficients are composed by the projections of lift and drag coefficients per blade length to the respective directions where ϕ is the flow angle defined as the angle between the local relative velocity and the rotor plane. The lift C_l and drag C_d coefficients per blade length depend on local airfoil profile and they are computed using 2D airfoil data as a function of angle of attack α and Reynolds number (Re). The relation between the local flow angle and local angle of attack is given by $\phi = \alpha + \beta$ where β is the sum of local twist angle θ_t and the pitch angle θ_p given by $\beta = \theta_p + \theta_t$. Moreover, The Re number of an airfoil profile is defined as $\mathrm{Re} = V_{rel}c/\nu$ where ν and c denote the kinematic viscosity of fluid and the chord length of an airfoil, respectively.

Figure 2 displays the velocity triangle formed locally at a cross-section of a rotor blade for the turbine configuration which results in new expressions for equations 3a and 3b as

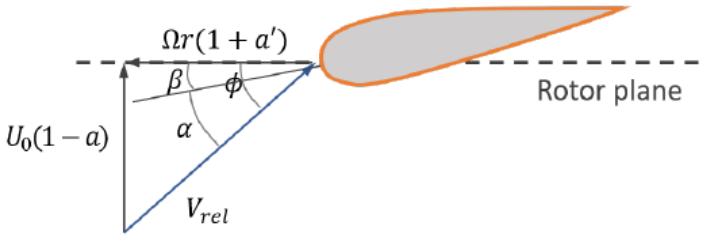

Figure 2. Turbine velocity triangle at the rotor plane [4].

$$\mathrm{dT} = \frac{1}{2}\rho Z c \frac{U_0^2\,(1-a)^2}{\sin^2(\phi)} C_n \mathrm{dr}, \tag{4a}$$

$$\mathrm{dQ} = \frac{1}{2}\rho Z c \frac{U_0\,(1-a)\,\Omega r\,(1+a)}{\sin\,(\phi)\cos\,(\phi)} C_t \mathrm{dr}, \tag{4b}$$

By combining equation 1 with equation 4a and equation 2 with equation 4b, the final expressions for the axial and tangential induction factors can be written as

$$a = \frac{1}{\dfrac{4\sin^2(\phi)}{\sigma C_n} + 1} \quad , \quad a' = \frac{1}{\dfrac{4\sin(\phi)\cos(\phi)}{\sigma C_t} - 1}, \tag{5}$$

where $\sigma = Zc/2\pi r$ denotes the local solidity as the portion of the annular area covered by the blades. The momentum theory can be extended to take into account the finite number of rotor blades by introducing the tip loss factor F proposed by Glauert [3]. This results in the following relations used for the axial and tangential factors as

$$a = \frac{1}{\dfrac{4F\sin^2(\phi)}{\sigma C_n} + 1} \quad , \quad a' = \frac{1}{\dfrac{4F\sin(\phi)\cos(\phi)}{\sigma C_t} - 1}. \tag{6}$$

$$F = \frac{2}{\pi}\cos^{-1}(\exp(-f)) \quad , \quad f = \frac{Z(R_{tip} - r)}{2r\sin(\phi)}. \tag{7}$$

In the BEM method, the assumption of no radial dependency for different annular elements makes us evaluate each blade section separately using an iterative method. For propellers, the same procedure as above, is used to obtain axial and tangential factors. The only difference for the propeller is that the axial flow velocity accelerates while it passes through the rotor. Contrary to the turbine, the induced tangential velocity at the rotor plane of a propeller has the same sign of rotation as the rotor blades.

2.2. Modification of BEM Method for CRPT Concept

Since the CRPT concept is enclosed by a confined tunnel or pipe, the conservation of mass gives a constant axial velocity flowing from upstream to downstream runners. Therefore, a deceleration of axial velocity introduced by the axial induction factor a in the classical BEM equations is no longer valid and it is assumed to be zero ($a = 0$). For the present CRPT machine (see figure 1), in pump mode the flow passes rotor 1 first whereas in the turbine mode, the flow passes rotor 2 first. For both operating modes, the incoming axial velocity U_0 does not change across the runners and it is assumed to be constant. The rotational speeds of the runners (Ω_1 and Ω_2) can also be different. Moreover, the tangential induction factors at each runner i.e., a_1' and a_2' are different and must be calculated.

Figures 3 and 4 demonstrate the velocity triangle at the rotor plane of runners 1 and 2 in the pump and turbine modes, respectively. In both operating modes, the incoming flow for the upstream runner is swirl free whereas for the downstream rotor it includes swirl induced by the upstream runner. Therefore, a new expression of tangential induction factor a_d' for the downstream runner must be introduced to take the upstream swirl into account.

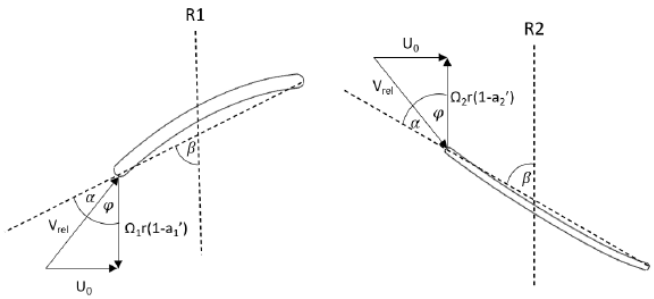

Figure 3. Velocity triangles of CRPT in pump mode.

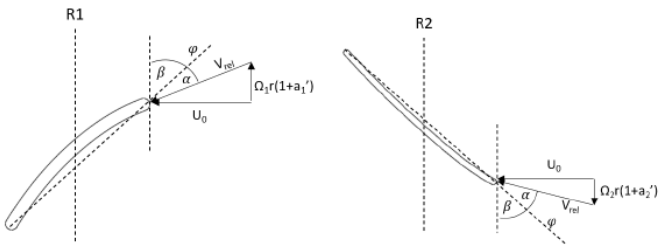

Figure 4. Velocity triangles of CRPT in turbine mode.

For this purpose, a linear interpolation approach as used in the classical BEM method for the induced tangential velocity at the rotor is used. This can be expressed as

$$u_{\theta,R} = u_{\theta,u} + \frac{(u_{\theta,d} - u_{\theta,u})}{2} = u_{\theta,u} + \frac{\Delta u_\theta}{2}, \tag{8}$$

where $u_{\theta,u}$, $u_{\theta,d}$, $u_{\theta,R}$ denote the tangential velocities before, after and at the rotor plane, respectively. Equation 8 can be re-written by replacing the upstream tangential velocity as $u_{\theta,u} = -2a'_u\Omega_u r$ and the tangential velocity at the downstream rotor as $u_{\theta,R} = a'_d\Omega_d r$ yielding the change of tangential velocity across the rotor as $\Delta u_\theta = 4a'_u\Omega_u r + 4a'_d\Omega_d r$. Therefore, the balance of angular momentum of an annular ring element can be re-written as

$$\mathrm{dQ}_d = r\Delta u_\theta \mathrm{d}\dot{m} = r(4a'_u\Omega_u r + 4a'_d\Omega_d r)\rho U_0 2\pi r \mathrm{dr}. \tag{9}$$

Equating equation 9 with the angular momentum obtained from the classical BEM theory (equation 4b) gives a modified induction factor for the downstream rotor as

$$a'_d = \frac{2k' a'_u \frac{\Omega_u}{\Omega_d} - 1}{-\frac{4F\sin(\phi_d)\cos(\phi_d)}{\sigma C_t} - C}, \tag{10}$$

where $C = 1$ and $C = -1$ are taken for the pump mode and turbine mode, respectively. Another modification for the CRPT concept, with respect to the original BEM method, is related to the static pressure discontinuity occurring across the rotor plane either as the pressure drop (for a turbine) or pressure jump (for a pump). The static pressure difference across the rotor plane in pump and turbine operational modes can be derived by subtraction of the total pressure before and after the rotor as

$$\Delta p_s = \begin{cases} \rho g \Delta H - \rho u_\theta^2/2 & \text{for pump,} \\ \rho g \Delta H + \rho u_\theta^2/2 & \text{for turbine,} \end{cases} \tag{11}$$

where ΔH and u_θ denote the total head difference and the flow tangential velocity after the rotor plane, respectively. The correction terms (which are then added to equations 3a and 3b) for the thrust and torque can be obtained by projecting of the static pressure difference at each blade element along the rotor given by

$$\mathrm{dT}_{corr} = \Delta p_s \cos(\beta) c \mathrm{dr} \quad , \quad \mathrm{dQ}_{corr} = \Delta p_s \sin(\beta) c \mathrm{dr}, \tag{12}$$

where β and c denote the twist angle and chord length of the blade element, respectively.

3. Numerical setup for Counter-Rotating Pump-Turbine machine

The numerical setup for the modified BEM method and CFD simulation of a CRPT as the validation case is explained in this section. RPTs based on the Francis turbine design, are widely used in the pumped-storage power plants [7]. However they have shown a limited performance in low-head scenarios where the height difference between both reservoirs is small. An axial shaft-driven CRPT configuration as displayed in figure 1 may be an alternative in such cases [8]. It can perform better than a conventional single rotor configuration for a wider range of operating conditions [9].

As seen in figure 5, in pump mode, the flow goes from left to right (runner 1 is the upstream runner) whereas in turbine mode, the flow goes from right to left (runner 2 is the upstream runner). In this study, a scaled CRPT model with runners diameters of 276 mm is used where runner 1 and runner 2 have eight and seven blades, respectively. In addition, each runner can rotate with different rotational speeds covering a broad range of operating conditions.

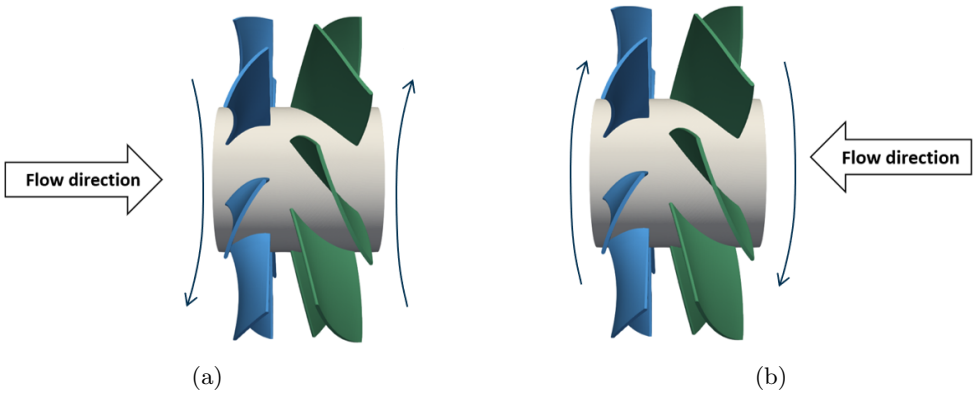

Figure 5. Flow and runner rotational directions, (a) pump and (b) turbine modes.

3.1. BEM Simulation Set-up

In the BEM method, the rotor blades are introduced as a collection of 2D airfoil profiles stacked at different radial positions along the pitch axis. In this study, to extract the airfoil profiles, each runner is divided into nine different profiles along the radial direction where the first profile is located near the hub and the last profile near the shroud. In the BEM calculations, the blade can be divided into a number of blade elements (In this study, the blade is divided into ten equally distributed blade elements where runner 1 and runner 2 have eight and seven blades, respectively). Therefore, the aerodynamic properties of any evaluation point along the blade can be obtained by interpolation between the blade profiles for a given angle of attack and Reynolds number. The extracted 2D profiles for both runners have special shapes, and there is no information about the lift (C_l) and drag (C_d) coefficients as a function of angle of attack (α) used in the BEM calculation. Therefore, a tabulated 2D airfoil table for each profile of the runners at different Reynolds number must be provided. This has been done through numerous steady-state CFD simulations using OpenFOAM-v1912 for moderate angle of attacks ranging from -15 to 15 degrees where the steady-state assumption is still valid. For higher angle of attacks, the Viterna extrapolation method has been used.

3.2. CFD Simulation of CRPT (Validation Case)

The developed BEM method for the CRPT concept is validated against incompressible CFD simulations using OpenFOAM (version FOAM-extend 4.1). This version allows for the use of a `mixingPlane` interface and the solver used is `MRFSimpleFoam` for steady-state simulation using multiple reference frames. Figure 6 displays the geometry used in the CFD simulation including both runners separated by a given distance. The interface located between the rotors is a `mixingPlane` interface computing circumferential averaged quantities. In addition, cyclic GGI boundary conditions on the sides are used to reduce the computational time while considering periodicity of the runners.

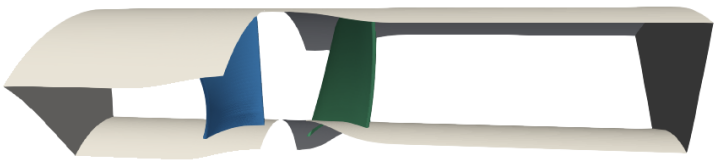

Figure 6. Schematic of runners 1 and 2 in the coupled CFD simulation set-up.

In the numerical simulations, the SIMPLE algorithm is used to couple pressure and velocity. To account for turbulence, the two equation eddy viscosity model k-ω SST (shear stress transport) turbulence model is employed. All variables are discretized using schemes of 2^{nd} order accuracy, except for the turbulent variables k and ω where the 1^{st} order accurate upwind scheme is used. The flow velocity is specified at the inlet of the computational domain, and a fixed pressure at the outlet.

4. Results and discussions

The developed BEM method is used to compute the blade loading, resulting in torque Q and thrust T for each runner, in both pump and turbine operating modes. The ratio of rotational speeds of runners 1 and 2 is assumed to be constant as $\Omega_2/\Omega_1 = 0.75$ for all simulations. Moreover, the results are presented using thrust coefficient CT and power coefficient P at various tip-speed ratios TSR (commonly used in wind power application) and they are defined as

$$\text{CT} = \frac{T}{\frac{1}{2}\rho A U_0^2} \quad , \quad \text{CP} = \frac{P}{\frac{1}{2}\rho A U_0^3} = \frac{Q\Omega}{\frac{1}{2}\rho A U_0^3} \quad , \quad \text{TSR} = \frac{\Omega R_{tip}}{U_0}. \tag{13}$$

where T, P, Q, A, U_0, Ω and R_{tip} denote the rotor thrust, rotor power, rotor torque, rotor area, upstream flow velocity and rotor (runner) radius, respectively. The thrust and torque of a rotor are computed by integrating the normal and tangential force at each blade element along the rotor, respectively. To study the impact of the tip loss factor F introduced in the classical BEM equations (see equation 6) and the extra loading due to the static pressure difference (see equation 12), four different types of BEM simulations are performed. They are labeled as `BEM`, `CORR`, `BEM_noF` and `CORR_noF`. The `BEM` case represents the original BEM method with Prandtl tip loss correction factor whereas in the `BEM_noF` case, the Prandtl tip loss correction factor is neglected. Similarly, the `CORR` case stands for the classical BEM modified by the extra loading because of the static pressure difference across the runners. Finally, `CORR_noF` case is obtained by omitting the Prandtl tip loss correction factor in the `CORR` case.

4.1. Pump Mode

In pump mode, as seen in figure 5(a), the flow direction is from left to right, first passing through runner 1 followed by runner 2. Runner 1 rotates in the clockwise direction whereas runner 2 rotates in the opposite direction, looking in the flow direction.

Figure 7 shows the thrust CT and power CP coefficients for various operating conditions expressed by the tip-speed ratio TSR for the upstream runner 1. As seen, neglecting the tip loss factor F in the BEM method increases the overall blade loading in both normal and tangential directions resulting in higher thrust and power coefficients, respectively.

For the downstream rotor, figure 8 displays the thrust CT and power CP coefficients at different tip-speed ratios. All BEM-based simulation cases predict a higher loading compared with the CFD simulations. However, both BEM and CFD simulations demonstrate similar trends for varying tip-speed ratios.

4.2. Turbine Mode

Contrary to the pump mode, as seen in figure 5(b), in the turbine mode the flow direction is from right to left. Runner 1 and runner 2 rotate clockwise and anti-clockwise, respectively while looking in the flow direction.

Figure 9 presents the thrust CT and power CP coefficients, obtained from the BEM and CFD simulations, for the upstream runner in the turbine operating mode. Similar to in pump mode, the modified BEM method including the static pressure correction term (indicated by

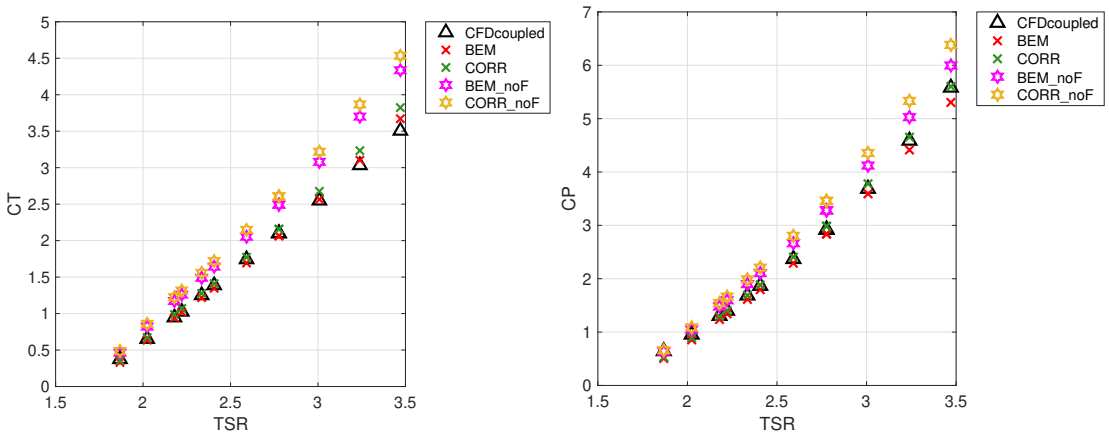

Figure 7. Power and thrust coefficients at various tip-speed ratios for runner 1 in pump mode.

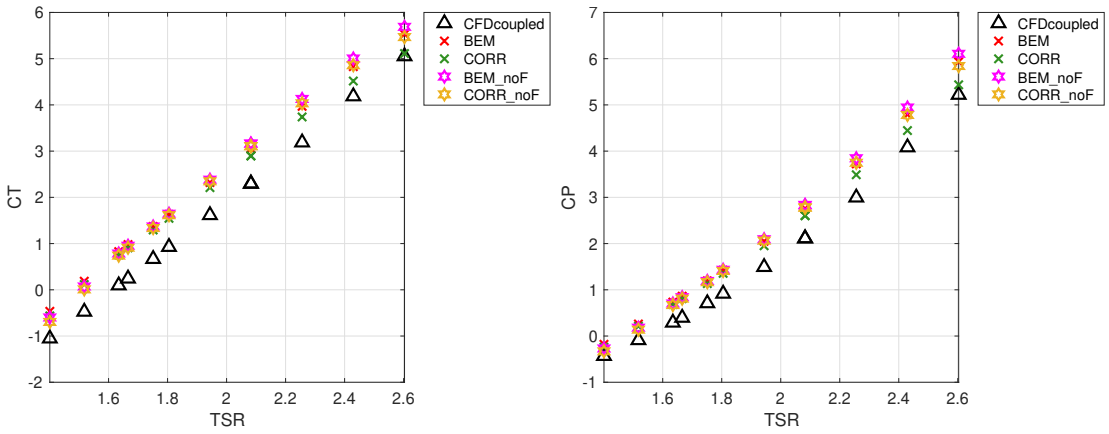

Figure 8. Power and thrust coefficients at various tip-speed ratios for runner 2 in pump mode.

`CORR`) increases the rotor loading. Moreover, neglecting the tip loss factor F (indicated by `noF`), similar to the pump mode, increases both thrust and power coefficients.

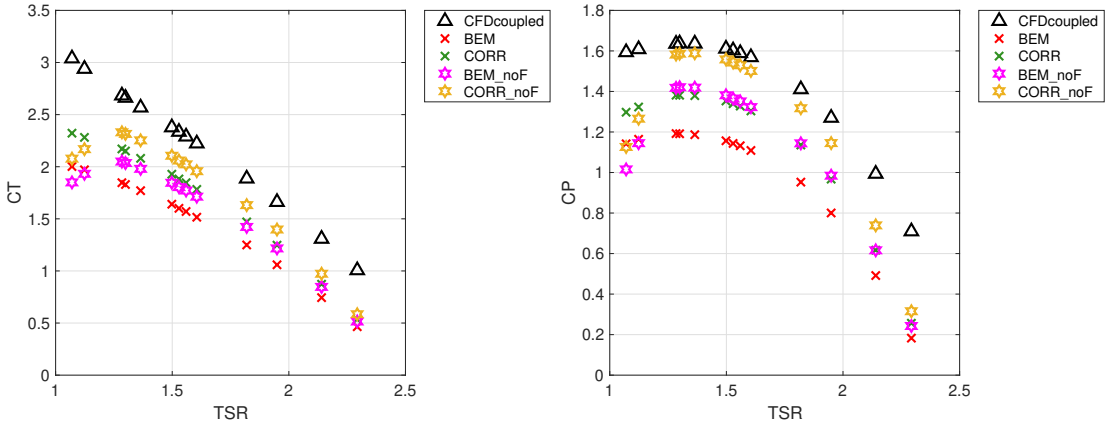

Figure 9. Power and thrust coefficients at various tip-speed ratios for runner 2 in turbine mode.

For the downstream runner in turbine mode, as seen in figure 10, the trend between the CFD

and BEM approaches is in a fairly good agreement, although the magnitude differs. Furthermore, the negative thrust and power coefficients occurring at higher tip-speed ratio implies infeasible operating conditions.

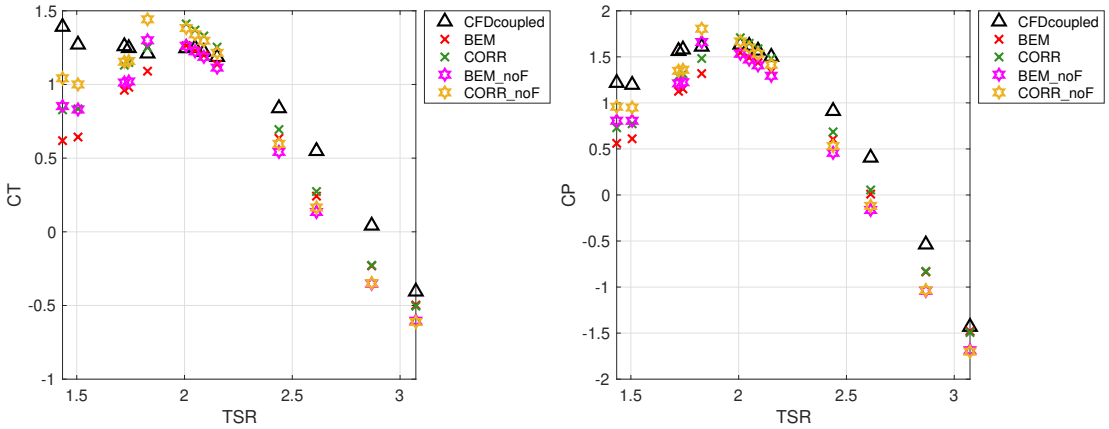

Figure 10. Power and thrust coefficients at various tip-speed ratios for runner 1 in turbine mode.

5. Conclusions

A successful implementation of the classical BEM method to predict the performance of a Counter-Rotating Pump-Turbine (CRPT) machine was presented. The results show that the modified BEM method can follow the same trend as CFD with some margin. In pump mode, neglecting tip loss factor F for both the upstream and downstream rotors increases the loading. In addition, the proposed correction that takes the static pressure difference across the runners into account increases the loading, especially for the downstream runner. This leads to an overestimation of the forces acting on the runners compared with the CFD results. In turbine mode, the offset between the BEM and CFD methods for the upstream runner is higher than in pump mode, where the BEM method predicts lower loading. In turbine mode, except for high tip-speed ratio, it was also shown that neglecting the tip loss correction factor F can increase the loading for the upstream runner. For the downstream runner, for a certain range of TSR, there is a fairly good agreement between the BEM and CFD results.

6. Acknowledgements

This project has received funding from the European Union's Horizon 2020 research and innovation programme under grant agreement No. 883553, and the "Swedish Hydropower Centre - SVC". SVC is established by the Swedish Energy Agency, EnergiForsk and Svenska Kraftnät together with Luleå University of Technology, The Royal Institute of Technology, Chalmers University of Technology and Uppsala University, www.svc.nu. The computations were enabled by resources provided by the Swedish National Infrastructure for Computing (SNIC) at Chalmers Centre for Computational Science and Engineering (C3SE) partially funded by the Swedish Research Council through grant agreement No. 2018-05973.

References

[1] Rankine W 1865 *Transaction of the Institute of Naval Architects* **6** 13–39
[2] Froude W 1878 *Transaction of the Institute of Naval Architects* **19** 22–33
[3] Glauert H 1935 Airplane propellers *Aerodynamic Theory* (Berlin, Heidelberg: Springer) https://doi.org/10.1007/978-3-642-91487-4_3

[4] Hansen M 2008 *Aerodynamics of Wind Turbines: second edition* 2nd ed (Earthscan) ISBN 978-1-84407-438-9
[5] Branlard E 2017 *Wind Turbine Aerodynamics and Vorticity-Based Methods: Fundamentals and Recent Applications* (Springer International Publishing) ISBN 978-3-319-55163-0
[6] Sørensen J N 2016 *General Momentum Theory for Horizontal Axis Wind Turbines* (Springer International Publishing) ISBN 978-3-319-22114-4
[7] Dixon S and Hall C 2014 *Fluid Mechanics and Thermodynamics of Turbomachinery* (Elsevier, Butterworth-Heinemann) ISBN 978-0-12-415954-9
[8] Hoffstaedt J P *et al.* 2022 *Renewable and Sustainable Energy Reviews* **158** 112119 ISSN 1364-0321
[9] Furukawa A, Shigemitsu T and Watanabe S 2007 *Journal of Thermal Science* **16** 7–13 ISSN 1003-2169